Article

Oxygenation of the Earth aided by mineral–organic carbon preservation

Mingyu Zhao [1,2] ✉, **Benjamin J. W. Mills** [1], **William B. Homoky** [1] & **Caroline L. Peacock** [1]

Photosynthesis produces molecular oxygen, but it is the burial of organic carbon in sediments that has allowed this O_2 to accumulate in Earth's atmosphere. Yet many direct controls on the preservation and burial of organic carbon have not been explored in detail. For modern Earth, it is known that reactive iron phases are important for organic carbon preservation, suggesting that the availability of particulate iron could be an important factor for the oxygenation of the oceans and atmosphere over Earth history. Here we develop a theoretical model to investigate the effect of mineral–organic preservation on the oxygenation of the Earth, supported by a proxy compilation for terrigenous inputs and the burial of reactive iron phases, and find that changes to the rate of iron input to the global ocean constitute an independent control on atmosphere–ocean O_2 and marine sulfate levels. We therefore suggest that increasing continental exposure and denudation may have helped fuel the rise in atmospheric O_2 and other oxidants over Earth history. Finally, we show that inclusion of mineral–organic preservation makes the global marine O_2 reservoir more resilient to changes in nutrient levels by breaking the link between productivity and organic carbon burial. We conclude that mineral–organic preservation is an important missing process in current assessments of Earth's long-term carbon cycle.

While photosynthesis is the proximate source of molecular oxygen, maintaining an oxidized atmosphere over geological time requires the burial of photosynthetically produced organic carbon (OC) in sediments, which prevents its re-reaction with O_2 (ref. [1]). Availability of the limiting nutrient phosphorus is believed to be the main driver for the production and thus the final burial of OC[2], and it is usually the supply of P that is considered to modulate atmospheric O_2 over Earth history[3–5]. In the modern ocean, however, only a minor amount (~13%) of OC that reaches the sediment is buried because the majority is microbially remineralized back into carbon dioxide[6].

The lack of a simple link between the export of biomass from the surface seawater and the long-term burial of OC in sediments raises questions about the connection between nutrient availability in the photic zone and long-term atmospheric oxygenation. It is reasonable to expect, therefore, that changes to the reactivity of OC, through either local temperature changes or the protection against microbial remineralization afforded to OC by binding with seafloor minerals[7–9], could be important for the geological O_2 cycle and may provide alternative explanations for the long-term rise in O_2 over Earth history. For example, many minerals that can bind OC are sourced from the continents and may therefore have undergone substantial increases in abundance over Earth history during continental emergence, with the potential to dramatically increase the preservation potential of OC and thus oxygenate the Earth.

The binding of OC with iron minerals, Fe (oxyhydr)oxides in particular, is a ubiquitous process in soils and sediments[7,10] in which Fe (oxyhydr)oxides can sequester OC in multiple ways, including via adsorption of OC onto mineral surfaces, coprecipitation of OC with

[1]School of Earth and Environment, University of Leeds, Leeds, UK. [2]Key Laboratory of Cenozoic Geology and Environment, Institute of Geology and Geophysics, Chinese Academy of Sciences, Beijing, China. ✉e-mail: mingyu.zhao@mail.iggcas.ac.cn

mineral particles and complexation between reactive Fe phases and OC to form macromolecules and nanoparticulate organominerals[11–13]. Through sequestration with Fe (oxyhydr)oxides, OC is less susceptible to chemical and microbiological attack[12,14,15]. In marine sediments, Fe reduction experiments show that 21.5 ± 8.6% of all OC is bound with reactive Fe phases, most likely via coprecipitation with Fe (oxyhydr)oxides and complexation to form macromolecules composed of OC and Fe (oxyhydr)oxide nanoparticles[7]. Reactive Fe phases are therefore invoked as a 'rusty sink' for OC that can protect bound carbon from microbial remineralization and enhance its long-term burial[7,16,17].

A global biogeochemical model with mineral OC burial

In this Article, we develop a global biogeochemical ocean–atmosphere–sediment model to test the effect that mineral protection of OC might have on the global carbon, O_2 and nutrient cycles. Specifically, we investigate how Fe mineral protection alters the relationship between limiting nutrient availability and carbon burial, and how changing the supply of Fe (oxyhydr)oxides would influence the long-term planetary redox state. We note that clay minerals may also have played a substantial role in OC preservation[18–20], and while we do not model this process, because both iron and clay minerals can be sourced from terrigenous material, they may further promote OC preservation when material delivery is high.

Our model is developed from a series of well-established conceptual models of global marine biogeochemistry[21–26]. The model tracks the global cycles of organic and inorganic carbon, sulfate and sulfide anions, Fe, O_2 and P in a five-box ocean system representing the shallow shelf, deep shelf, surface open ocean, surface high latitude and deep ocean and has explicit air–sea exchange with a single well-mixed atmosphere box (Fig. 1 and Supplementary Fig. 1). The majority of fluxes and other process information is taken directly from these previous works and adapted onto our six-box scheme. To calibrate the model using known geological records, carbonate precipitation and the cycling of carbon isotopes are also included in the model.

The dissolved Fe in all ocean boxes is divided into Fe(II) and Fe(III) (Fig. 1). The input fluxes of dissolved Fe to the ocean are the riverine influx of dissolved Fe(III), the release of dissolved Fe(III) to the surface ocean due to dissolution of dust, the hydrothermal dissolved Fe(II) flux and the benthic dissolved Fe(II) flux generated by Fe reduction in the sediments. Dissolved Fe is free to redistribute around the ocean via circulation and mixing between ocean boxes. The reaction pathways for the Fe cycle in the ocean boxes are taken to be Fe reduction, pyrite formation, siderite precipitation, aerobic Fe oxidation and Fe(III) scavenging by particles (the formation of nanoparticulate Fe (oxyhydr)oxides, which aggrade with other particles and sink to the sediments), following recent works by Wallmann et al.[24] and van de Velde et al.[26]. Another flux of Fe (oxyhydr)oxides to the sediments is the weathering and transport of particulate Fe directly from land (through both river and dust; Fig. 1).

Primary production in all three surface oceanic boxes is determined by P and Fe concentrations through nutrient co-limitation[24]. The degradation of OC in the water column is determined by the availability of electron acceptors in the priority order of O_2, Fe(III), SO_4^{2-} (refs. [26,27]). We have added a mineral-protected OC burial term in sediments to mimic OC burial due to the protection by Fe (oxyhydr)oxides. This is done by dividing the burial of OC into two parts: mineral-protected OC burial associated with Fe (oxyhydr)oxides and unprotected OC that is degraded through the cascade of electron acceptors. Following the findings of Lalonde et al.[7], we have parameterized the fraction of OC burial associated with Fe (oxyhydr)oxides using a fixed OC/Fe ratio in the range of 4 ± 2. Due to this ratio, the net effect of Fe(II) and/or Fe(III) input into seawater, if buried as Fe (oxyhydr)oxides, is expected to be an increase in O_2 level in the ocean and atmosphere system[16]. The OC burial that
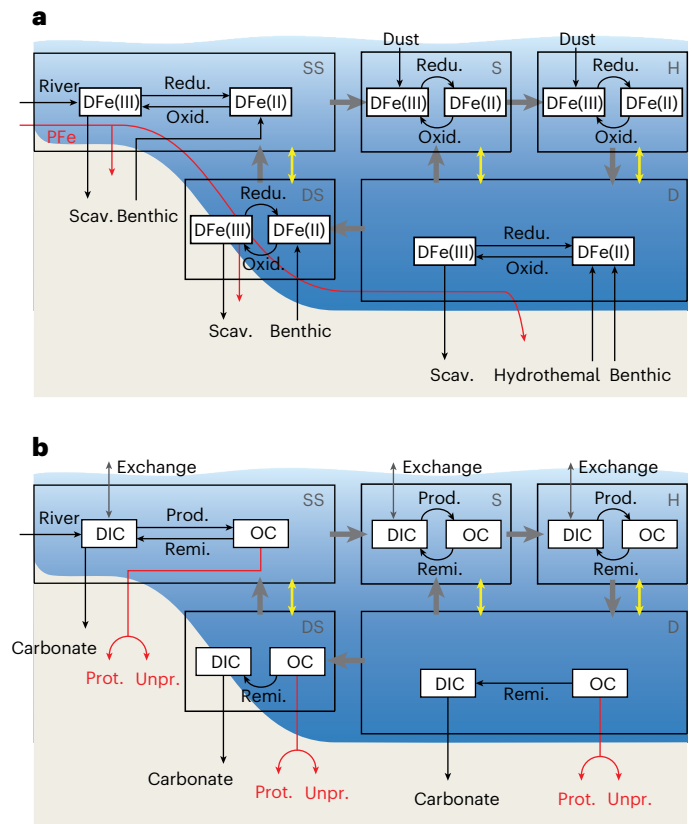
Fig. 1 | Schematic diagram of the global biogeochemical model. a, Iron cycle. Dissolved iron in water bodies exists as dissolved Fe(II) (DFe(II)) or Fe(III) (DFe(III)). A terrigenous source of particulate Fe(III) (oxyhydr)oxides (PFe) is also supplied to marine sediments. b, Carbon cycle. Carbon in the oceanic reservoirs exists as dissolved inorganic carbon (DIC) or OC. Boxes with a blue background represent oceanic reservoirs. White boxes represent reservoirs of chemical components, grey arrows represent thermohaline transport fluxes and yellow arrows represent mixing fluxes. SS, shallow shelf; DS, deep shelf; S, surface open ocean; H, surface high latitude; D, deep ocean. Redu., reduction; Oxid., oxidation; Scav., scavenging. Prod., production; Remi., remineralization; Prot., OC protected by Fe(III) (oxyhydr)oxides; Unpr., OC unprotected.

is not associated with Fe (oxyhydr)oxides is calculated using a fixed burial efficiency, following the majority of previous work[25,28]. Oxidative weathering of fossil OC on land is described as a function of O_2 level[29].

Our model is constructed around the assumption of a present-day steady state, but we also validate its general function by testing it in a simulation of the Permian–Triassic boundary (Supplementary Fig. 2). During this time, the emplacement of the Siberian Traps Large Igneous Province resulted in an extreme CO_2 input event, which is well documented through shifts in ocean acidity, carbon burial systematics and ocean oxygenation[25,30–32]. Our model produces a reasonable fit to the changes in ocean pH and carbonate $\delta^{13}C$ across the carbon input event[32] and predicts a notable reduction in marine O_2 concentration and a rise in water-column H_2S concentration. Thus, we conclude it represents the long-term carbon and O_2 cycles in a manner consistent with current scientific understanding. The longer-term recovery in our model is slower than in ref. [32], probably because we do not impose changes to erosion rates or enhanced weathering of igneous rocks. The full model outline and computer code is included in Supplementary Information.

An independent driver for Earth's oxygenation

Figure 2 shows the key steady states of our model under changes to the weathering input of dissolved P (x axis) and co-varying fluxes of

a

b

c
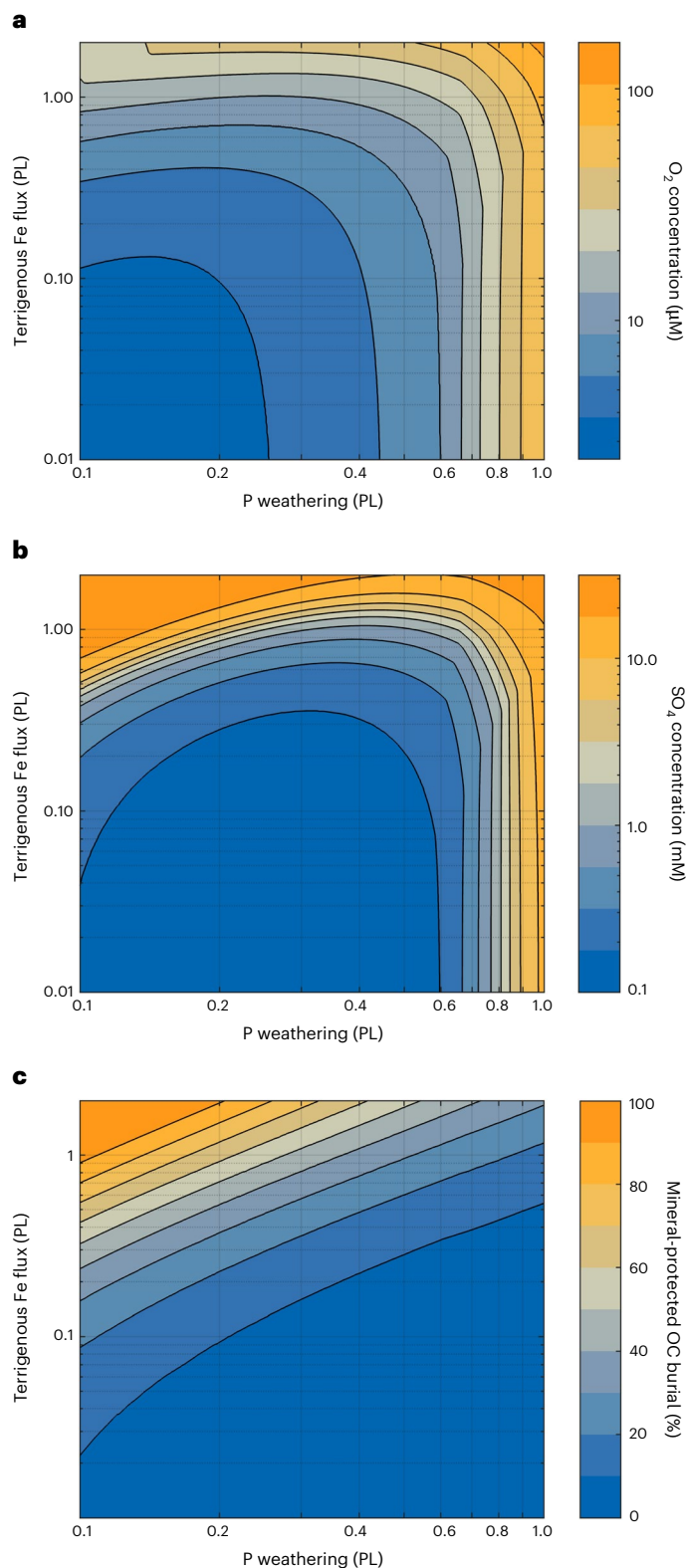
Fig. 2 | Influence of Fe and P delivery to the ocean on OC burial and the oceanic redox state under mineral protection of OC. a, O_2 concentration in the deep ocean. **b**, SO_4 concentration in the deep ocean. **c**, Percentage of mineral-protected OC burial in total OC burial. PL, present level.

particulate Fe (oxyhydr)oxides from rivers and dissolved Fe(III) from the dissolution of dust—collectively termed 'terrigenous Fe flux' (*y* axis). A decoupling between P and Fe inputs to the ocean may be achieved

because Fe and P can be hosted in different minerals in igneous rocks, such as feldspar and apatite, with different susceptibilities to dissolution and transport. Therefore, a change in weathering regime—the relative intensities of physical and chemical weathering processes—or dust flux may alter the proportions of Fe and P delivered to the ocean from the continents.

Here the burial of OC associated with Fe (oxyhydr)oxides increases with an increase in the terrigenous Fe flux because the overall delivery of Fe to sediments is greater. This results in increased amounts of O_2 and SO_4 in the model ocean because more OC is protected by Fe and therefore less of the oxidized species are consumed during remineralization. The effects of this mechanism can cause O_2 levels averaged across the model boxes to vary by one to two orders of magnitude for a similar variation in the Fe flux. The effects are also greater when P weathering inputs are lower because this results in a reduced flux of OC to sediments and therefore a proportionally greater protected fraction of OC (Fig. 2c).

As in previous studies, our model continues to show that increasing P availability, and therefore photosynthetic gross primary production (Supplementary Fig. 4), can drive increased dissolved O_2 and SO_4 in the oceans[33,34], but our analysis adds two important pieces of information to this general view. First, supply of Fe to the oceans, and the direct effect of this on mineral preservation and OC burial, constitutes an independent control on electron acceptor availability, which may also drive large changes in marine O_2 and SO_4 concentrations. Second, changes in P availability may have a substantially different effect depending on the Fe supply flux. When Fe supply is high, a reduction in P availability may not drive a large reduction in oxidant availability (for example, top right of Fig. 2a,b) as previous models have predicted[35]. Supplementary Figs. 5–7 show model sensitivity tests where we rerun Fig. 2 under a different rate of ocean circulation, input of sulfate and degree of redox-dependent P recycling. These figures confirm that the overall behaviour of the model shown in Fig. 2 is robust to these considerations.

Empirical evidence

Geological evidence is consistent with our hypothesis that the variations in Fe delivery from the continents may have played an important role in the evolution of ocean–atmosphere O_2 (Fig. 3). To estimate the broad changes in Fe (oxyhydr)oxide delivery to the oceans over Earth history, we consider the increase in exposed continental land area over time and plot the elevation of active continental crust and the normalized strontium isotope curve[36,37], which are expected to track changes in overall terrigenous delivery from the continents to the oceans and thus changes in Fe (oxyhydr)oxide delivery as a fraction of terrigenous material. Such an enhancement of continental erosion may have acted as the root driver for the increase in OC burial associated with Fe (oxyhydr)oxides and, thus, atmospheric oxygenation.

Although there is large uncertainty in the estimation of the evolution of land area with time[38–40], most models show a substantial increase in land masses during 3.0–2.3 billion years ago (Ga), and between the Archaean and Palaeoproterozoic the strontium isotope record shows a drift towards higher values, consistent with increased continentally sourced Sr[36] (Fig. 3). Continental elevation and strontium isotope records are also consistent with further increases in material delivery during 1000–500 million years ago (Ma) (Fig. 3). Between 3.0 and 2.3 Ga, the emergence of land masses probably brought substantial terrigenous material to seawater and hence substantial amounts of Fe, which is also consistent with the occurrence of major Fe formations after 2.75 Ga (ref. [41]; Fig. 3). This Fe influx corresponds with the Great Oxygenation Event (~2.4–2.2 Ga) and multiple independent lines of evidence for 'whiffs' of O_2 before it[42,43]. Between 1000 and 500 Ma, the further increases in continental elevation and terrigenous inputs correspond with the Neoproterozoic Oxygenation Event (~800–550 Ma)[36,37]. We therefore suggest that an increase in terrigenous inputs into the
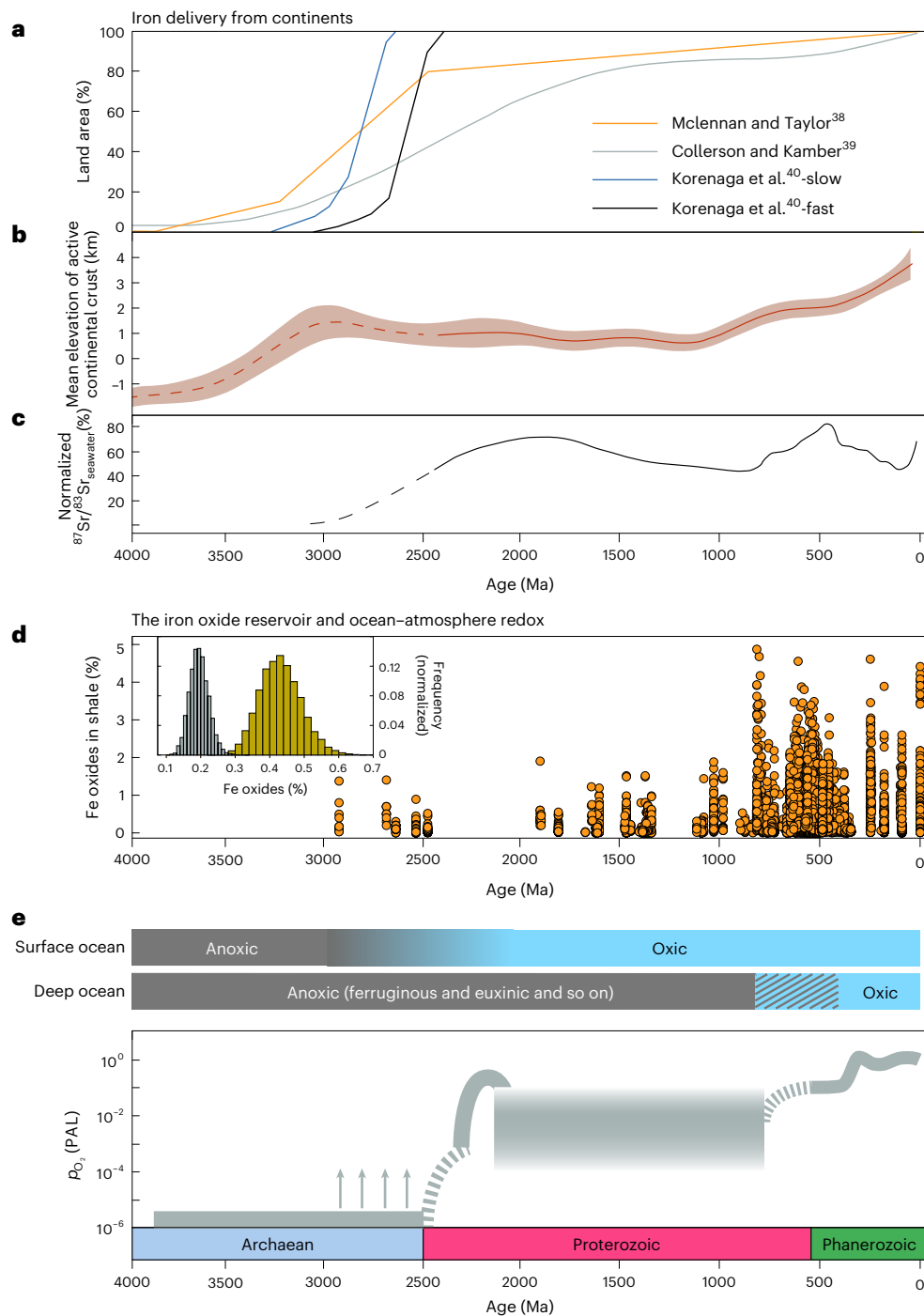
Fig. 3 | The evolution of Fe fluxes, oceanic redox and atmospheric p_{O_2}. a, The evolution of continental area. The results of ref. [40] for fast and slow plate tectonics are based on the continental growth model of ref. [45]. **b**, Mean elevation of active continental crust based on records of zircon europium anomaly[37]. The shadow represents a 95% confidence interval. **c**, Normalized $^{87}Sr/^{86}Sr$ curve of continental weathering versus mantle influence[36], where normalization removes the effects of ^{87}Rb decay over Earth history. **d**, The evolution of concentration of Fe (oxyhydr)

oxides in shale through time (see Supplementary Information for the description of data compiling). The panel on the upper left shows the frequency distributions of bootstrap resampled mean concentrations of Fe (oxyhydr)oxides in shale ($n = 10{,}000$) before 830 Ma (grey) and after 830 Ma (green). **e**, Current understanding of the evolution of atmospheric p_{O_2} relative to present atmospheric level (PAL), after ref. [33]. The oceanic redox in **e** is adapted from ref. [5].

ocean and an associated increase in the terrigenous Fe flux may have resulted in substantial OC burial, contributing to the oxygenation of the ocean and atmospheric system. While we focus on iron in this Article, the evidence here also supports the potential for a wider link between terrigenous material delivery and Earth's oxygenation, which may also include other minerals and processes.

It is difficult to track the global burial rate of Fe (oxyhydr)oxides directly. This is because sedimentary concentrations can reflect Fe transport in the ocean as well as redox-dependent conversion of Fe oxides to authigenic minerals such as pyrite. A compiled dataset (see Supplementary Information for the description of the compilation) for the content of Fe (oxyhydr)oxides in shales shows a particularly

substantial increase during the Neoproterozoic Oxygenation Event (Fig. 3). The mean content of Fe (oxyhydr)oxides of post-Tonian age (<830 Ma) is more than twice that of the pre-Cryogenian (>830 Ma)—0.43 ± 0.12 wt% versus 0.19 ± 0.06 wt% (2 s.d.). The unpaired Student's t test shows that the difference between these two mean values is significant ($P < 0.001$, $\alpha = 0.01$), and the increase in mean contents of Fe (oxyhydr)oxides remains robust during bootstrap resampling (Fig. 3). This increase in the abundance of Fe (oxyhydr)oxides may have been driven by the progressive oxygenation of the ocean interior during the late Precambrian. If so, then this may constitute a positive-feedback regime where more OC is mineral preserved, which drives further oxygenation (for example, Supplementary Fig. 8).

We conclude that mineral protection of OC, driven by supply of Fe from the continents, probably has been an independent driver of increased marine O_2 and SO_4 concentrations and has led to a system that is more resilient to deoxygenation by restriction of P supply to the oceans. This adds weight to the hypothesis that the ultimate driver of Earth's oxygenation is the emergence and/or uplift of continental land masses[38,43,44], a process that in our model would raise atmospheric p_{O_2} and marine O_2 and SO_4 levels and buffer the system against collapses in biological productivity. We suggest that the direct effect of Fe minerals on OC preservation and burial should be included in subsequent analyses of the long-term oxygenation of Earth.

Online content

Any methods, additional references, Nature Portfolio reporting summaries, source data, extended data, supplementary information, acknowledgements, peer review information; details of author contributions and competing interests; and statements of data and code availability are available at https://doi.org/10.1038/s41561-023-01133-2.

References

1. Garrels, R. M. Cycling of carbon, sulfur, and oxygen through geologic time. *Sea* **5**, 303–336 (1974).
2. Tyrrell, T. The relative influences of nitrogen and phosphorus on oceanic primary production. *Nature* **400**, 525–531 (1999).
3. Bjerrum, C. J. & Canfield, D. E. Ocean productivity before about 1.9 Gyr ago limited by phosphorus adsorption onto iron oxides. *Nature* **417**, 159–162 (2002).
4. Reinhard, C. T. et al. Evolution of the global phosphorus cycle. *Nature* **541**, 386–389 (2017).
5. Alcott, L. J., Mills, B. J. W. & Poulton, S. W. Stepwise Earth oxygenation is an inherent property of global biogeochemical cycling. *Science* **366**, 1333–1337 (2019).
6. Burdige, D. J. Preservation of organic matter in marine sediments: controls, mechanisms, and an imbalance in sediment organic carbon budgets? *Chem. Rev.* **107**, 467–485 (2007).
7. Lalonde, K., Mucci, A., Ouellet, A. & Gelinas, Y. Preservation of organic matter in sediments promoted by iron. *Nature* **483**, 198–200 (2012).
8. Arndt, S. et al. Quantifying the degradation of organic matter in marine sediments: a review and synthesis. *Earth Sci. Rev.* **123**, 53–86 (2013).
9. Hemingway, J. D. et al. Mineral protection regulates long-term global preservation of natural organic carbon. *Nature* **570**, 228–231 (2019).
10. Wagai, R. & Mayer, L. M. Sorptive stabilization of organic matter in soils by hydrous iron oxides. *Geochim. Cosmochim. Acta* **71**, 25–35 (2007).
11. Eusterhues, K. et al. Characterization of ferrihydrite–soil organic matter coprecipitates by X-ray diffraction and Mossbauer spectroscopy. *Environ. Sci. Technol.* **42**, 7891–7897 (2008).
12. Curti, L. et al. Carboxyl-richness controls organic carbon preservation during coprecipitation with iron (oxyhydr)oxides in the natural environment. *Commun. Earth Environ.* **2**, 229 (2021).
13. Homoky, W. B. et al. Iron colloids dominate sedimentary supply to the ocean interior. *Proc. Natl Acad. Sci. USA* **118**, e2016078118 (2021).
14. Eusterhues, K., Neidhardt, J., Hädrich, A., Küsel, K. & Kai, U. T. Biodegradation of ferrihydrite-associated organic matter. *Biogeochemistry* **119**, 45–50 (2014).
15. Xiao, K. Q., Moore, O. W., Babakhani, P., Curti, L. & Peacock, C. L. Mineralogical control on methylotrophic methanogenesis and implications for cryptic methane cycling in marine surface sediment. *Nat. Commun.* **13**, 2722 (2022).
16. Barber, A. et al. Preservation of organic matter in marine sediments by inner-sphere interactions with reactive iron. *Sci. Rep.* **7**, 366 (2017).
17. Eglinton, T. I. A rusty carbon sink. *Nature* **483**, 165–166 (2012).
18. Emerson, S. R. & Hedges, J. I. Sediment diagenesis and benthic flux. *Treatise Geochem.* **6**, 293–319 (2003).
19. Kennedy, M., Droser, M., Mayer, L. M., Pevear, D. & Mrofka, D. Late Precambrian oxygenation; inception of the clay mineral factory. *Science* **311**, 1446–1449 (2006).
20. Blattmann, T. M. et al. Mineralogical control on the fate of continentally derived organic matter in the ocean. *Science* **366**, 7742–7745 (2019).
21. Wallmann, K. Feedbacks between oceanic redox states and marine productivity: a model perspective focused on benthic phosphorus cycling. *Glob. Biogeochem. Cycles* **17**, 1084 (2003).
22. Slomp, C. & Cappellen, Van P. The global marine phosphorus cycle: sensitivity to oceanic circulation. *Biogeosciences* **4**, 155–171 (2007).
23. Zeebe, R. E. LOSCAR: long-term ocean–atmosphere–sediment carbon cycle reservoir model v.2.0.4. *Geosci. Model Dev.* **5**, 149–166 (2012).
24. Wallmann, K. et al. Periodic changes in the Cretaceous ocean and climate caused by marine redox see-saw. *Nat. Geosci.* **12**, 456–461 (2019).
25. Dal Corso, J. et al. Permo–Triassic boundary carbon and mercury cycling linked to terrestrial ecosystem collapse. *Nat. Commun.* **11**, 2962 (2020).
26. van de Velde, S. J., Hülse, D., Reinhard, C. T. & Ridgwell, A. Anoxic iron and sulphur cycling in the cGENIE.muffin Earth system model (v.0.9.16). *Geosci. Model Dev. Discuss.* **2020**, 1–44 (2020).
27. Froelich, P. N. et al. Early oxidation of organic matter in pelagic sediments of the eastern equatorial Atlantic: suboxic diagenesis. *Geochim. Cosmochim. Acta* **43**, 1075–1090 (1979).
28. Lenton, T. M., Daines, S. J. & Mills, B. J. COPSE reloaded: an improved model of biogeochemical cycling over Phanerozoic time. *Earth Sci. Rev.* **178**, 1–28 (2018).
29. Bolton, E. W., Berner, R. A. & Petsch, S. T. The weathering of sedimentary organic matter as a control on atmospheric O_2: II. Theoretical modeling. *Am. J. Sci.* **306**, 575–615 (2006).
30. Magaritz, M. & Holser, W. T. The Permian–Triassic of the Gartnerkofel-1 core (Carnic Alps, Austria): carbon and oxygen isotope variations. *Abh. Geol. B-A* **45**, 149–163 (1991).
31. Lau, K. V. et al. Marine anoxia and delayed Earth system recovery after the end-Permian extinction. *Proc. Natl Acad. Sci. USA* **113**, 2360–2365 (2016).
32. Jurikova, H. et al. Permian–Triassic mass extinction pulses driven by major marine carbon cycle perturbations. *Nat. Geosci.* **13**, 745–750 (2020).
33. Lyons, T. W., Reinhard, C. T. & Planavsky, N. J. The rise of oxygen in Earth's early ocean and atmosphere. *Nature* **506**, 307–315 (2014).
34. Kah, L. C., Lyons, T. W. & Frank, T. D. Low marine sulphate and protracted oxygenation of the Proterozoic biosphere. *Nature* **431**, 834–838 (2004).

35. Laakso, T. A. & Schrag, D. P. Regulation of atmospheric oxygen during the Proterozoic. *Earth Planet. Sci. Lett.* **388**, 81–91 (2014).

36. Shields, G. A. A normalised seawater strontium isotope curve: possible implications for Neoproterozoic–Cambrian weathering rates and the further oxygenation of the Earth. *eEarth* **2**, 35–42 (2007).

37. Tang, M., Chu, X., Hao, J. & Shen, B. Orogenic quiescence in Earth's middle age. *Science* **371**, 728–731 (2021).

38. McLennan, S. M. & Taylor, S. Geochemical constraints on the growth of the continental crust. *J. Geol.* **90**, 347–361 (1982).

39. Collerson, K. D. & Kamber, B. S. Evolution of the continents and the atmosphere inferred from Th–U–Nb systematics of the depleted mantle. *Science* **283**, 1519–1522 (1999).

40. Korenaga, J., Planavsky, N. J. & Evans, D. A. D. Global water cycle and the coevolution of the Earth's interior and surface environment. *Phil. Trans. R. Soc. A* **375**, 20150393 (2017).

41. Konhauser, K. et al. Iron formations: a global record of Neoarchean to Palaeoproterozoic environmental history. *Earth Sci. Rev.* **172**, 140–177 (2017).

42. Anbar, A. D. et al. A whiff of oxygen before the great oxidation event? *Science* **317**, 1903–1906 (2007).

43. Ostrander, C. M. et al. Fully oxygenated water columns over continental shelves before the Great Oxidation Event. *Nat. Geosci.* **12**, 186–191 (2019).

44. Godderis, Y. & Veizer, J. Tectonic control of chemical and isotopic composition of ancient oceans: the impact of continental growth. *Am. J. Sci.* **300**, 434–461 (2000).

45. Armstrong, R. L. Radiogenic isotopes: the case for crustal recycling on a near-steady-state no-continental-growth Earth. *Phil. Trans. R. Soc. A* **301**, 443–472 (1981).

Methods

Model structure

Our model is developed from a series of well-established conceptual models of global biogeochemical cycles[21–26,28]. The model has five ocean boxes (Supplementary Fig. 1): shallow margin (sm), deep margin (dm), surface (s), surface high latitude (h) and deep (d). Following the results of ref. [46], the shallow-margin box is defined from 0–100 m water depth and occupies 10% of the ocean surface and 5% of the seafloor. The deep-margin box is 100–1,000 m water depth and occupies a further 5% of the seafloor. The surface box is 100 m deep and represents 76.5% of the ocean surface, while the surface high-latitude box is 250 m deep and represents 13.5% of the ocean surface. The species, fluxes, main equations, parameters and reactions in the model are shown in Supplementary Tables 1–4. Supplementary Table 1 shows the model species and their sizes at present (based on refs. [5,21,22,25,47–54]), Supplementary Table 2 shows the chemical/biological reactions, Supplementary Table 3 shows the flux equations and Supplementary Table 4 shows the model parameters. A schematic of the model structure is shown in Supplementary Fig. 1. The following sections explain key reactions and burial fluxes of the model. See Supplementary Information for a more detailed description of the model.

Reactions

The model approximates the main reactions of C, O, S and Fe cycles in the water column (Supplementary Table 2). These reactions include photosynthesis, aerobic degradation of organic matter, iron reduction, sulfate reduction, pyrite formation, aerobic iron oxidation, aerobic sulfide oxidation, sulfide-mediated iron reduction, siderite formation and Fe(III) scavenging. The reaction rate laws of photosynthesis and respiration are discussed below. See Supplementary Information for the description of all the reactions in the model.

Primary production in the surface boxes ($Pripr_i$) is calculated considering nutrient co-limitation by P and Fe[24]:

$$Pripr_i = K_{PP_i} \times \min\left[C_{DP_i} \times \frac{C_{DP_i}}{C_{DP_i} + K_P}, \frac{C_{FeIII_i}}{r_{FeP}} \times \frac{C_{FeIII_i}}{C_{FeIII_i} + K_{Fe}} \right] \quad (1)$$

where K_{PPi} is the kinetic constant of primary productivity in box i, C_{DP_i} is the P concentration in box i, C_{FeIII_i} is the Fe(III) concentration in box i, r_{FeP} is the atomic ratio between Fe and P in phytoplankton biomass, and K_P and K_{Fe} are Monod constants.

The rates for the pathways of organic matter degradation via aerobic respiration (AR_i), iron reduction ($ironR_i$) and sulfate reduction ($sulfR_i$) are calculated using a Monod scheme[55,56] as the sequence of these pathways is controlled by their energy yields[27]. Thus, the reaction rate laws of these pathways are:

$$AR_i = K_{Remin_i} \times C_{POC_i} \times \frac{C_{O2_i}}{C_{O2_i} + K_{O2}} \quad (2)$$

$$ironR_i = K_{Remin_i} \times C_{POC_i} \times \frac{K_{O2}}{C_{O2_i} + K_{O2}} \times \frac{C_{FeIII_i}}{C_{FeIII_i} + K_{FeIII}} \quad (3)$$

$$sulfR_i = \Psi \times K_{Remin_i} \times C_{POC_i} \times \frac{K_{O2}}{C_{O2_i} + K_{O2}} \times \frac{K_{FeIII}}{C_{FeIII_i} + K_{FeIII}} \times \frac{C_{SO4_i}}{C_{SO4_i} + K_{SO4}} \quad (4)$$

where K_{Remin_i} is the rate constant for organic matter degradation in box i, C_{POC_i} is the concentration of particulate OC (POC) in box i, C_{O2_i} is the concentration of oxygen in box i, C_{FeIII_i} is the concentration of Fe(III) in box i, C_{SO4_i} is the concentration of SO_4^{2-} in box i, Ψ is the attenuation factor for sulfate reduction, K_{O2} is the limiting concentration for aerobic respiration and K_{FeIII} is the limiting concentration for

iron reduction. The total remineralization rate ($Remin_i$) in each ocean box is the sum of aerobic respiration (AR_i), iron reduction ($ironR_i$) and sulfate reduction ($sulfR_i$):

$$Remin_i = AR_i + ironR_i + sulfR_i \quad (5)$$

Burial fluxes

The modern burial fluxes of OC in the shallow margin ($f_{mocb_{sm}}$), deep margin ($f_{mocb_{dm}}$) and deep sea (f_{mocb_d}) are set as 4.5 Tmol yr^{-1}, 1.5 Tmol yr^{-1} and 1 Tmol yr^{-1}, respectively, following ref. [22]. This also follows the findings of ref. [57] that roughly 20% of the marine OC burial occurs in the deep sea. The modern POC fluxes to the sediment–seawater interface in the shallow margin (Sed_{sm}) and deep margin (Sed_{dm}) are estimated to be 30 Tmol yr^{-1} and 10 Tmol yr^{-1} using $f_{mocb_{sm}}$, $f_{mocb_{dm}}$ and assuming a burial efficiency (BE) of ~15 % for the sediments on the continental margin[6]. Similarly, the modern POC flux to the sediment–seawater interface in the deep ocean (Sed_d) is estimated to be 10 Tmol yr^{-1} using f_{mocb_d} and a BE of ~10% for the deep-ocean sediments[6]. The OC burial is divided into two parts: OC burial associated with Fe and 'unprotected' OC burial. The OC burial fluxes associated with Fe ($f_{mocb_i}^{Fe}$) are estimated using the burial flux of Fe and an OC: Fe burial ratio (γ_{OCFe}^b; ref. [7]) such that:

$$f_{mocb_{sm}}^{Fe} = \gamma_{OCFe}^b \times \left(f_{FeIIIsolid_{sm}} + f_{FeIIIscaveng_{sm}} - f_{beniFeII_{sm}} \right) \quad (6)$$

$$f_{mocb_{dm}}^{Fe} = \gamma_{OCFe}^b \times \left(f_{FeIIIsolid_{dm}} + f_{FeIIIscaveng_{dm}} - f_{beniFeII_{dm}} \right) \quad (7)$$

$$f_{mocb_d}^{Fe} = \gamma_{OCFe}^b \times \left(f_{FeIIIsolid_d} + f_{FeIIIscaveng_s} + f_{FeIIIscaveng_h} + f_{FeIIIscaveng_d} - f_{beniFeII_d} \right) \quad (8)$$

where $f_{FeIIIsolid_i}$ represents the particulate Fe(III) flux from continental weathering, and $f_{beniFeII_d}$ represents the benthic flux of Fe(II). The burial fluxes of OC (f_{mocb_i}) are therefore calculated as:

$$f_{mocb_i} = \begin{cases} f_{mocb_i}^{Fe} + \left(Sed_i - f_{mocb_i}^{Fe} \right) \times BEO_i, Sed_i > f_{mocb_i}^{Fe} \\ Sed_i, Sed_i < f_{mocb_i}^{Fe} \end{cases} \quad (9)$$

where BEO_i represents BE of organic matter that is not associated with Fe. BEO_i is calculated using modern values of f_{mocb_i}, $f_{mocb_i}^{Fe}$ and Sed_i.

The burial flux of sulfate as evaporites in the shallow-margin box (f_{SO4b}) is scaled with sulfate concentration[28]:

$$f_{SO4b} = k_{SO4b} \times \frac{C_{SO4_{sm}}}{C_{SO4_{sm0}}} \quad (10)$$

where f_{SO4b} is the present burial flux of sulfate in the shallow-margin box.

The P burial fluxes include three components: organic P, iron-bound P and authigenic P. The burial fluxes of organic P ($POPbur_i$) are scaled with the burial fluxes of organic matter using a fixed C/P ratio in marine sediments (γ_{CP}^b):

$$POPbur_i = f_{mocb_i}/\gamma_{CP}^b \quad (11)$$

The burial flux of iron-bound P (FeP_i) is scaled with the P concentration (DP_i) in the oceanic box that is in contact with sediments:

$$FeP_i = kFeP_i \times DP_i/DP_{i_0} \quad (12)$$

where DP_{i_0} is the initial dissolved P concentration in oceanic box i. The burial flux of authigenic P ($Pauth_i$) is also scaled with seawater P concentration:

$$Pauth_i = kPauth_i \times DP_i/DP_{i_0} \qquad (13)$$

Model testing

We test the model behaviour by running a large perturbation experiment from Earth history−the Permian−Triassic carbon injection from the Siberian Traps. The purpose of this is to test whether the model is consistent with previous modelling approaches−we do not make any conclusions on the Permian−Triassic. Here the CO_2 injection flux and isotopic composition follow recent modelling work using a similar type of model[32]. The response of our model to this flux (Supplementary Fig. 2) compares well to the recent modelling work and to the geological record for carbonate $\delta^{13}C$ and marine pH. Our model also produces marine deoxygenation and an increase in the amount of free sulfide in the water column[31,58,59]. We also run a test of a large P input flux roughly modelled on an often-hypothesized trigger for the Cretaceous ocean anoxic events (Supplementary Fig. 3). The model outputs for this event show deoxygenation and a positive carbon isotope excursion, again generally consistent with the prevailing views on the global biogeochemical response to massive P inputs[60]. We conclude in this section that our model behaviour in response to changes in carbon and nutrient cycles is broadly in line with other modelling efforts and with current understanding of Earth's biogeochemical functions.

Data availability

The compiled data on the contents of Fe (oxyhydr)oxides in shale are available at the online version of this paper.

Code availability

The processing MATLAB codes are available at the online version of this paper.

References

46. Costello, M. J., Cheung, A. & De Hauwere, N. Surface area and the seabed area, volume, depth, slope, and topographic variation for the world's seas, oceans, and countries. *Environ. Sci. Technol.* **44**, 8821–8828 (2010).

47. Schlitzer, R. et al. The GEOTRACES intermediate data product 2017. *Chem. Geol.* **493**, 210–223 (2018).

48. Martiny, A. C. et al. Biogeochemical controls of surface ocean phosphate. *Sci. Adv.* **5**, eaax0341 (2019).

49. Levitus, S., Conkright, M. E., Reid, J. L., Najjar, R. G. & Mantyla, A. Distribution of nitrate, phosphate and silicate in the world oceans. *Prog. Oceanogr.* **31**, 245–273 (1993).

50. Anderson, L. A. & Sarmiento, J. L. Global ocean phosphate and oxygen simulations. *Glob. Biogeochem. Cycles* **9**, 621–636 (1995).

51. Chinni, V., Singh, S. K., Bhushan, R., Rengarajan, R. & Sarma, V. Spatial variability in dissolved iron concentrations in the marginal and open waters of the Indian Ocean. *Mar. Chem.* **208**, 11–28 (2019).

52. Tagliabue, A. et al. A global compilation of dissolved iron measurements: focus on distributions and processes in the Southern Ocean. *Biogeosciences* **9**, 2333–2349 (2012).

53. Boyd, P. W. & Ellwood, M. J. The biogeochemical cycle of iron in the ocean. *Nat. Geosci.* **3**, 675–682 (2010).

54. Bottrell, S. H. & Newton, R. J. Reconstruction of changes in global sulfur cycling from marine sulfate isotopes. *Earth Sci. Rev.* **75**, 59–83 (2006).

55. Reed, D. C., Slomp, C. P. & Gustafsson, B. G. Sedimentary phosphorus dynamics and the evolution of bottom-water hypoxia: a coupled benthic–pelagic model of a coastal system. *Limnol. Oceanogr.* **56**, 1075–1092 (2011).

56. Zhao, M., Zhang, S., Tarhan, L. G., Reinhard, C. T. & Planavsky, N. The role of calcium in regulating marine phosphorus burial and atmospheric oxygenation. *Nat. Commun.* **11**, 2232 (2020).

57. Berner, R. A. Burial of organic carbon and pyrite sulfur in the modern ocean: its geochemical and environmental significance. *Am. J. Sci.* **282**, 451–473 (1982).

58. Zhang, G. et al. Redox chemistry changes in the Panthalassic Ocean linked to the end-Permian mass extinction and delayed Early Triassic biotic recovery. *Proc. Natl Acad. Sci. USA* **114**, 1806–1810 (2017).

59. Zhang, F. et al. Congruent Permian–Triassic $\delta^{238}U$ records at Panthalassic and Tethyan sites: confirmation of global-oceanic anoxia and validation of the U-isotope paleoredox proxy. *Geology* **46**, 327–330 (2018).

60. Tsandev, I. & Slomp, C. Modeling phosphorus cycling and carbon burial during Cretaceous Oceanic Anoxic Events. *Earth Planet. Sci. Lett.* **286**, 71–79 (2009).

Author contributions

C.L.P., B.J.W.M. and W.B.H. conceived the paper. All authors were involved in the discussion on the model construction, simulations and results. M.Z. and B.J.W.M. wrote the model code, with significant input from C.L.P. and W.B.H.

Competing interests

The authors declare no competing interests.

Additional information

Supplementary information The online version contains supplementary material available at https://doi.org/10.1038/s41561-023-01133-2.

Correspondence and requests for materials should be addressed to Mingyu Zhao.

Peer review information *Nature Geoscience* thanks Florian Scholz and Francois Clayer for their contribution to the peer review of this work. Primary Handling Editors: Rebecca Neely and Tom Richardson, in collaboration with the *Nature Geoscience* team.

Reprints and permissions information is available at www.nature.com/reprints.